crystals

MDPI

Article

Assessment of the Durability Dynamics of High-Performance Concrete Blended with a Fibrous Rice Husk Ash

David O. Nduka [1,*], Babatunde J. Olawuyi [2], Olabosipo I. Fagbenle [1] and Belén G. Fonteboa [3]

[1] Department of Building Technology, College of Science and Technology, Km. 10 Idiroko Road, Covenant University, Ota 112233, Nigeria; olabosipo.fagbenle@covenantunivesity.edu.ng
[2] Department of Building, School of Environmental Technology, Federal University of Technology, Minna 920211, Nigeria; babatunde@futminna.edu.ng
[3] Department of Civil Engineering, School of Civil Engineering, University of A Coruña, 15001 A Coruña, Spain; belen.gonzalez.fonteboa@udc.es
* Correspondence: david.nduka@covenantuniversity.edu.ng

Abstract: The present study examines the durability properties of Class 1 (50–75 MPa) high-performance concrete (HPC) blended with rice husk ash (RHA) as a partial replacement of CEM II B-L, 42.5 N. Six HPC mixes were prepared with RHA and used as 5%, 10%, 15%, 20%, 25%, and 30% of CEM II alone and properties are compared with control mix having only CEM II. The binders (CEM II and RHA) were investigated for particle size distribution (PSD), specific surface area (SSA), oxide compositions, mineralogical phases, morphology, and functional groups using advanced techniques of laser PSD, Brunauer–Emmett–Teller (BET), X-ray fluorescence (XRF), X-ray diffraction (XRD), scanning electron microscopy (SEM), and Fourier transform infrared/attenuated total reflection (FTIR/ATR), respectively, to understand their import on HPC. Durability properties, including water absorption, sorptivity, and chemical attack of the HPC samples, were investigated to realise the effect of RHA on the HPC matrix. The findings revealed that the durability properties of RHA-based HPCs exhibited an acceptable range of values consistent with relevant standards. The findings established that self-produced RHA would be beneficial as a cement replacement in HPC. As the RHA is a cost-effective agro-waste, a scalable product of RHA would be a resource for sustainable technology.

Keywords: durability properties; high-performance concrete; rice husk ash; superabsorbent polymers; sustainability

Citation: Nduka, D.O.; Olawuyi, B.J.; Fagbenle, O.I.; Fonteboa, B.G. Assessment of the Durability Dynamics of High-Performance Concrete Blended with a Fibrous Rice Husk Ash. *Crystals* **2022**, *12*, 75. https://doi.org/10.3390/cryst12010075

Academic Editors: Shima Pilehvar and Luís G. Baltazar

Received: 23 November 2021
Accepted: 11 December 2021
Published: 6 January 2022

1. Introduction

The construction industry contributes significantly to any economy, and its components are vital to advancing socio-economic development goals of shelter, infrastructure, employment, and improved well-being [1]. However, the industry has a long history of negatively affecting the environment and human health. For instance, Rheude et al. [2] attributed high energy consumption, depletion of natural resources, high global anthropogenic CO_2 emissions, waste generation, and air pollution to construction industry activities. Notwithstanding the environmental menaces, Rheude et al. [2] further pointed out that the construction sector is poised to build more urban space in the coming 40 years than in the last 4000 years due to increasing population and urbanisation. The architecture, engineering, and construction (AEC) projects require cement, a major constituent of mortar and concrete cum basic and widely used building material. Adekoya [3] projected Nigeria's local cement production capacity to hit 60 million metric tonnes per annum (MMT/a) by 2022. The report further revealed that key players in Nigeria's cement production, including Dangote Cement PLC, has an installed capacity of 29.3 MMT/a, followed by Lafarge Africa PLC at 10.5 MMT/a and BUA Group, which stands at 9 MMT/a with expected plans to increase to 20 MMT/a at the end of 2022. The rise in cement production in Nigeria will continue to increase 0.870 $GtCO_2$ emissions recorded in 2015 [4]. Nigeria's

cement production sector largely contributes to the estimated 8% of the total anthropogenic CO_2 emission from the global cement production [5] during the clinkerisation process of converting calcium carbonate into lime at approximately 1450 °C.

Among the various strategies to reduce greenhouse gases, especially CO_2, clinker substitution, i.e., replacing carbon-intensive clinker with supplementary cementitious materials (SCMs), is one of the four major pillars for global carbon emission reduction protocols. There are economic and environmental sustainability benefits accrued from SCMs incorporation in a cement matrix. Zhang et al. [6] posit that approximately 25–30% reduction of CO_2 emissions can be achieved via cement replacement with SCMs. In the same vein, Oyebisi et al. [4] stress that the absence of SCMs in many concrete structures developed in the 20th and 21st centuries led to their deterioration between the first and second decades of development. SCMs are noted to react and deplete the calcium hydroxide in cement composite to form calcium silicate hydrate (C-S-H) gel responsible for more strength development of concrete [6,7]. Hossain et al. [7] experimentally showed that SCMs-based concrete demonstrates excellent or equivalent physical, mechanical, durability, and microstructural properties compared to Portland cement.

In this respect, the continuous rise in urbanisation and industrialisation worldwide has demanded concrete with better strength and durability properties in super tall buildings and heavy civil engineering projects [6]. These AEC structural projects require high-performance concrete (HPC) with better compressive, flexural, and tensile strengths, and improved durability to resist attacking ions like chloride/sulphate or chemical agents. HPC is traditionally described as concrete with improved strength, workability, and durability performance, which cannot be attained with usual materials through standard mixing, placing, and curing techniques [8–10]. The authors agreed that HPC has more cement content than the normal strength concrete, including one or more SCMs like silica fume (SF), fly ash (FA), ground granulated blast furnace slag (GGBS), metakaolin (MK), and calcined clay (CC), rice husk ash (RHA), etc. It is achieved by lowering the water to binder ratio (W/B) between 0.2–0.38 [11] and refining the pore structure and microstructure of cement paste with SCMs. At the same time, workability is improved with a large dose of superplasticiser [12,13]. The materials used are generally thoroughly picked superior quality constituents with an optimised mix design. The aggregates have to be robust, durable, and consistent with cement paste for stiffness and strength. The adoption of HPC is an effective measure to reduce the structural element's sizes without affecting the load-carrying capacity [6]. According to Zhang et al. [6], HPC technology saves usable space in buildings, reducing the dead load on structures with further minimisation of foundation size and cost. Irrespective of the wide use of fly ash, silica fume, metakaolin, etc., as a cement substitute in HPCs, RHA is gaining traction, especially in rice-producing countries [14,15].

The addition of RHA as an SCM in the cement matrix looks attractive to managing the large quantity of waste, especially in Nigeria, with rice production growth of approximately 70% in the last decade [16]. Ugbede et al. [17] reported that rice production in Nigeria increased from 5.5 million tonnes in 2015 to 5.8 million tonnes in 2017, with a 5% annual increase following federal government intervention policy on agriculture and economic development. For every one-tonne rice paddy, approximately 40 kg of rice husk presents environmental problems from widespread land occupation and disposal burning [18]. Rice husk is a by-product of rice production, and its high silicon content makes it difficult to degrade naturally [15]. It is mostly utilised as a fuel in electric generation, firing of clay bricks, and rice processing plants. About 20% of rice husk converts to RHA through open field burning or a controlled incinerator system, for which temperature and duration are either monitored or not [19,20]. Adnan et al. [20] considered rice husk to be typically preeminent in ash compared to other biomass fuels. A highly reactive RHA particle size and surface area depends on the controlling temperature and burning environment the rice husk is subjected to. The attractive property of RHA in blended cement comes from 87–97% of non-crystalline silica content, which is fibrous and lightweight, with an external

high surface area [20]. The addition of RHA brings about denser microstructure and homogeneity in concrete, preventing water and influencing chloride/sulphate ions and chemical agent migration [18]. Consequently, Hu et al. [21] reported a compressive increase of 11.3% at 28 days of hydration with a 15% replacement ratio with a high reactive RHA.

From the above, the use of highly reactive RHA with well-graded size distribution and low W/B in a blended cement matrix can achieve a close microstructure and improved durability in HPC. HPC is optimally designed with various fine materials, leading to a very dense microstructure and low permeability. The low transport of moisture and attacking ions impermeability generally improves the durability performances of HPC. Typical durability evaluation of RHA-based cement blend has been determined through chloride and sulphate ion penetration, acid attack, carbonation, shrinkage, sorptivity, porosity, and water absorption resistance tests. Rumman et al. [14] evaluated the chloride permeability resistance of high strength concrete at varied cement contents of 500, 425 and 350 kg/m^3 by RHA contents of 0, 55 and 70 kg/m^3, respectively. The W/B was fixed at 0.4 and 0.5 for each mix to propose a new mix design method that incorporates durability as a design factor and RHA as an SCM. Their results revealed that up to 20% RHA content, chloride permeability was reduced to approximately 63%. Hossain et al. [7] investigated the water absorption and sorptivity of a high strength mortar containing RHA as an SCM. A mix ratio of 1:3, with W/B of 0.4 and 0.5 at 5–20% cement replacement of five steps, was adopted. The hardened mortar samples were subjected to two different curing schemes (standard and high-temperature curing) for 1, 7, and 28 days. The water absorption and sorptivity test results revealed that RHA blended mortar with a high-temperature curing method showed an overall decline in water absorption and sorptivity.

Sahoo et al. [18] assessed the durability properties (water permeability, sorptivity, porosity, chloride permeability, carbonation resistance, and weight loss due to acid attack) of a normal strength concrete blended with RHA. At 15% RHA content cured for 28 and 60 days, sulphur acid attack reduced by 7% whereas the water permeability reduced by 15% at 90 days. The carbonation resistance result showed approximately 0.13 cm/day$^{0.5}$ in the magnitude of co-efficient of carbonation at 90 days. Chloride ion penetration recorded a reduction of approximately 15% at 10% RHA content, whereas 15% RHA content increased to 26.1%. Similarly, De Silva et al. [19] examined the effect of waste RHA residual ash from rice husk fueled brick kilns on the durability properties of a plastering mortar. With 550 kg/m^3 cement content, RHA was varied from 5–10% in five steps. Their finding showed a reduction of 54% and 70% in sulphate exposure for 5% and 10% RHA content. Weight loss in an alkaline environment reduced from 3.13% to 2.4% in 10–15% RHA content. Swaminathan et al. [22] investigated the influence of a ternary mix of Portland cement, metakaolin, and RHA on the durability properties of an M60 grade HPC. Their results revealed that the durability dimensions of water absorption, sorptivity, porosity, and permeability penetration improved due to RHA's presence in the mixture. Finally, Wang et al. [15], in their review of RHA performance on cement-based materials under various W/B, pointed out within 10–25% RHA content, chloride penetration resistance is optimised, carbonation resistance best improved at 20%, and shrinkage resistance optimisation stands at approximately 10–20% cement replacement. Wang et al. [15] placed sulphate resistance optimisation at 40 and 50% RHA content in the cementitious material. Generally, the authors noted that tested concrete and mortar samples' durability and mechanical properties improved within 10% and 20% of RHA content.

RHA has attracted a lot of research on the strength properties of normal strength concrete and mortar. However, few studies are available on durability dimensions of HPC, especially in developing countries like Nigeria. Hence this study investigates the durability properties of water absorption, sorptivity, and chemical attack of a fibrous RHA blended in HPC mixtures. The aim is to understand the feasibility of incorporating a controlled incinerated RHA into an HPC matrix in fulfilling its long-term durability properties. The information will be relevant for further RHA use in sustainable construction materials and the industry's growth.

2. Materials and Methods

2.1. Materials

2.1.1. Binders

Portland-limestone cement (CEM II B-L, 42.5 N) conforming to BS EN 197-1 [23] and NIS 444-1 [24] is used as the main binder in the current experiment. Here, RHA is used as a replacement for CEM II and produced in a controlled incinerator at 700 °C for 1 h in an electric furnace and pulverised using a grinding mill at Laboratory of Nigeria Cereals Research Institute, Baddegi, near Bida in Niger State, Nigeria. The workability of the HPC samples was improved using Masterglenium Sky 504—a polycarboxylic ether polymer-based superplasticiser supplied by BASF Limited (Lagos, Nigeria) and used within the manufacturer's best specification of $\leq$2% weight of binder (b_{wob}). The internal curing agent of superabsorbent polymers (SAP) tagged "FLOSET 27CC $\geq$ 300 µm" was added at fixed content of 0.3% by b_{wob}. The particle size distribution (PSD) and specific surface area of the binders were measured via the laser PSD (Malvern Mastersizer 3000, Worcestershire, UK) and Brunauer–Emmett–Teller, BET (Nova Station B Quantachrome Instrument, Boynton Beach, FL, USA) methods. Oxide compositions, mineralogical phases, and the morphology of the binders were analysed using X-ray fluorescence, XRF (Bruker AXS S4, Explorer, Karlsruhe, Germany), X-ray diffraction, XRD (Rigaku Miniflex 600, Washington, DC, USA), and scanning electron microscopy, SEM (Phenom ProX, PhenomWorld, Eindhoven, The Netherlands) techniques, respectively. The functional groups were investigated with Fourier transform infrared/attenuated total reflection, FTIR/ATR (Cary 630, Agilent Technologies, Penang, Malaysia).

2.1.2. Aggregates

Dry-conditioned river sand with a nearest particle size of 300 µm was used as fine aggregate in the experimental study [9,25]. Similarly, a 13.50 mm crushed granite stone retained on a 9.50 mm sieve size served as a coarse aggregate [9,26]. The coarse aggregate was washed to remove compromising materials and implemented at saturated surface dry condition. The mechanical and physical properties of the aggregates were also analysed for PSD (standard sieves), specific gravity, water absorption, aggregate crushing, and impact values.

2.1.3. Water

Portable water devoid of any toxic and floating materials and complying with BS EN 1008 [27] was used to prepare the HPCs.

2.2. HPC Mix Design

In line with the goal of this experimental work, seven variant mixtures inclusive of a control mix were designed. The control mix was designed for 28-day Class 1 (50–75 MPa) HPC having characteristic cube strength of 67 MPa, following the British method of HPC design. The other six HPCs mixtures were designed by replacing 5%, 10%, 15%, 20%, 25%, and 30% with RHA. A fixed 0.3 and 0.3% for W/B and SAP content by b_{wob} was maintained, respectively, and superplasticiser content of 1.5% b_{wob} was added for all the HPC mixtures to improve the workability. Added water of 12.5 g/g of SAP was furnished for the SAP permeability on the basis of the work of Olawuyi [28]. Each constituent of HPC was measured by weight (kg/m^3), and hence, the RHA additive was taken to be by weight of the binder. The HPC assemblies were labelled with the name "RHAC" and the replacement level. For instance, the HPC having RHA with 5% replacement was implied as RHAC-5. The details of the number of materials computed for all the seven HPC mixtures and their mix identifications are presented in Table 1.

Table 1. Mix Constituents of HPC with RHA.

Mix ID	Water (kg/m^3)	Cement-CEM II (kg/m^3)	RHA (kg/m^3)	Coarse Aggregate (kg/m^3)	Sand (kg/m^3)	SAP (0.3% b_{wob}) (kg/m^3)	Superplastiser (1.5% b_{wob}) (kg/m^3)	Water/Binder (W/B) (kg/m^3)	Extra Water (kg/m^3)
Control	156	540	0	1050	700	1.62	8.10	0.3	20.30
RHAC-5	156	513	27	1050	700	1.62	8.10	0.3	20.30
RHAC-10	156	486	54	1050	700	1.62	8.10	0.3	20.30
RHAC-15	156	459	81	1050	700	1.62	8.10	0.3	20.30
RHAC-20	156	432	108	1050	700	1.62	8.10	0.3	20.30
RHAC-25	156	405	135	1050	700	1.62	8.10	0.3	20.30
RHAC-30	156	378	162	1050	700	1.62	8.10	0.3	20.30

2.3. Production of Fresh HPC, Sample Casting, and Curing

Having obtained the required materials, they were mixed in a 50 litre pan-mixer to obtain a uniform workable mix. First, the fine aggregate followed by the binders were mixed in the pan-mixer for 1 min. Next, dry SAP particles were added, and all the fine contents were mixed for another 30 s. After that, the coarse aggregate was introduced, and mixing was maintained for 1 min before water previously mixed with superplasticiser was added. Finally, the mixing was sustained for an additional 3 min to obtain a harmonised workable fresh HPC mix, as proposed in the literature [28,29]. The fresh HPC was later undertaken for workability test via the slump flow. After fulfilling the workability standards fixed at 450 mm–600 mm flow value [9], the fresh HPC was poured into various previously oiled moulds of specified sizes. The specimens for the various tests were cast in two layers on a vibrating table. The cast samples were then protected in the laboratory with thick vapour barriers and allowed to harden for 24 h before demoulding, and they were then left to cure in a water tank at 20 ± 3 °C until the required curing ages (7, 28, 56 and 90, days respectively) before testing in accordance to standards [30–33].

2.4. Testing Procedures

The details concerning the specimen type, testing age, and standard followed for each test developed in the experimental study is provided in Table 2. The water absorption was examined on 100 mm size cubes following EN, B. 1097-6 [31]. The HPC samples were initially immersed in water for 28, 56, and 90 days with their weight obtained and tagged M_{wet}. After that, the samples were oven-dried at 110 ± 5 °C in triplicates pending a stable weight for 24 h. The dry samples were left to cool and then measured and recorded, denoted as M_{dry}. The water absorption value was analysed by subtracting the dry samples' weight from the saturated sample, dividing the result by the dry sample's weight, and multiplying by 100. Mathematically, water absorption, WA, value can be expressed as in Equation (1):

$$\frac{\text{Mwet} - \text{Mdry}}{\text{Mdry}} \times 100 \quad (1)$$

where WA (%) is the water absorption value; M_{wet} is the wet sample's weight; and M_{dry} is the dry sample's weight.

In the same vein, for investigating the water sorptivity test, water was allowed via a face of the Ø100 × 50 mm disc specimen under capillary action in line with ASTM C1585-04 [30]. First, the disc samples in triplicates were oven-dried at 110 ± 5 °C until reaching a fixed weight for 24 h. The discs were weighed again before dipping in approximately 30 mm of water. Samples were kept there for approximately 7 h, and data were recorded after 5, 10, 15, 30, 60, 120, and 180 min. The samples were then removed and weighed again to observe the amount of absorbed water. Equation (2) shows the results:

$$I = S.t^{0.5} \quad (2)$$

where I represents the cumulative ingress of water in mm, S is the sorptivity coefficient, and t, min is the sample's immersion time in the water. The mass of water absorbed into the specimen was converted into the volume. The volume of water plotted against the square root of time gives a straight line. The sorptivity coefficient was calculated by measuring the slope of this straight line. A best-fitted line was then computed using a regression analysis of data points for every HPC mix. The slope of the best-fitted line was the rate of absorption for that mixture.

Table 2. Details of tests and the specimen.

Test Conducted	Code Referred	Testing Age (days)	Sample Size
Water absorption test	EN, B. 1097-6 (2013)	28, 56 and 90	100 mm cubes
Water Sorptivity test	ASTM C1585-04 (2007)	28, 56 and 90	Ø100 × 50 mm disc
Chemical attack test (acid, sulphate, and chlorine resistances)	ASTM C267-20 (2020)	7, 28, 56 and 90	100 mm cubes
Compressive strength test	BS EN 12390-3 (2019)	7, 28, 56 and 90	100 mm cubes

The chemical attack of the HPCs was evaluated by immersing the specimen in 5% hydrochloric acid (HCl), 5% sodium sulphate (Na_2SO_4), and 5% calcium chloride ($CaCl_2$) solutions, respectively. The pH of the acidic, chloride, and sulphate environments were studied during the testing cycle. The solutions were renewed every 30 days after checking the pH of the solutions. The specimens were removed at 7, 28, 56, and 90 days after being exposed to acid, chloride, and sulphate solutions and washed with water. The effects of acid, chloride, and sulphate attack were evaluated based on compressive strength assessment. The compressive strength followed BS EN 12390-3 [32] and RILEM Technical Recommendation TC14-CPC 4 [34]. The HPC cubes were investigated using the Model YES-2000 digitised Materials Testing Machine (Eccles Technical Engineering Ltd., England, UK) with a 2000 kN maximum loading capacity.

3. Results

3.1. Characterisation of Binders

3.1.1. Physical Properties of Binders

Figure 1 shows that 90% (D_{90}) of CEM II and RHA particles are smaller than 4000 and 3900 nm, respectively. The median particle size, D_{50} of CEM II and RHA is 48.8 and 3200 nm, respectively. Furthermore, the particle size below 10% (D_{10}) falls within 4.88 and 160 nm, respectively, for the same samples. From Table 3, the SSA measured via the MultiPoint BET model showed 8.182 × 10^2 and 4.649 × 10^2 m^2/g for CEM II and RHA, respectively. The pore diameter of the binders analysed through the DA BET mode indicated corresponding values of 2.92 and 1.52 nm for CEM II and RHA samples. Based on these values, CEM II particles are finer than RHA particle size with a surface area close to each other. The physical properties of CEM II is available at [11]. Comparing the two binder's DA BET analysis, the RHA sample has a lower pore size diameter, conforming to macro-mesoporous material [35] and the SSA conforming to Kwan and Wong [36].

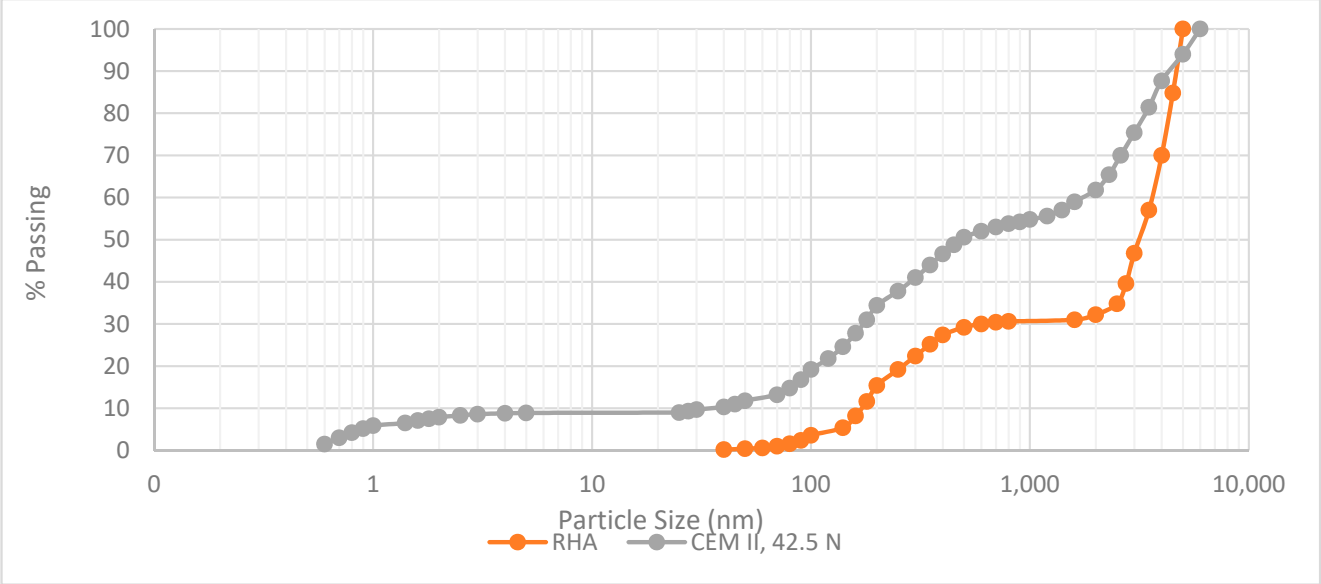

Figure 1. Particle size distribution of binders.

Table 3. Physical properties of binder materials. (Nduka et al., 2021).

Properties	CEM II	RHA
Specific gravity	3.12	2.15
MultiPoint BET specific surface area (m^2/g)	8.182×10^2	4.649×10^2
Soundness (%)	0.75	-
Initial and final setting times (min)	90 and 205	-
Pore diameter mode-DA (nm)	2.92	1.52
D_{90}	4000	3900
D_{50}	48.8	3200
D_{10}	4.88	160

3.1.2. Chemical Composition of Binders

The results in Table 4 inform the choice of the SCM having functional oxides (SiO_2 + Al_2O_3 + Fe_2O_3) of 82.62% and conform to ASTM Standard C 618 [37]. The chemical composition of CEM II is available at [11] study. The total amount of silica, alumina, and iron oxide required for mineral admixture's amorphousness is rated to be above 70%. This standard only guides mineral admixtures' potential reactivity [38]. RHA here contains 80% SiO_2, 1.8% Al_2O_3, 0.8% Fe_2O_3, and 0.8% CaO. It can be noticed that the Fe_2O_3 of CEM II (3.19) was greater than the RHA (0.79), which could be responsible for the higher specific gravity and density. However, the oxide percentage of RHA depends on the type, source, origin, and calcination systems. CEM II contains CaO and SiO_2 of approximately 57% and 15%, respectively. The CaO and SiO_2 oxide percentage values obtained here are below the limits of 60–67% (CaO) and 17–25% (SiO_2), respectively, recommended by Newman and Choo [39] for 42.5 N cement class. There exists a 9.18% difference in the useful chemical oxides found in the RHA used in the present study and those reviewed by Mosaberpanah and Umar [40]. For example, they found the average useful oxides of SiO_2, Al_2O_2, and Fe_2O_2 in RHA in India, Vietnam, Malaysia, Brazil, and the USA to be 90.98%. Therefore, RHA's chemical oxide composition generally conforms to class N of ASTM C 618 [37] minimum requirements for possible pozzolans.

Table 4. Chemical composition of CEM II and RHA. (Nduka et al., 2021).

Oxides	SiO_2	Al_2O_3	Fe_2O_3	CaO	MgO	SO_3	K_2O	Na_2O	M_2O_5	P_2O_5	TiO_2	LOI
RHA (%)	80.02	1.81	0.79	0.82	0.74	0.08	1.01	0.00	0.26	4.31	0.43	10.62
CEM II (%)	15.38	4.14	3.19	56.92	2.44	1.59	0.21	0.04	0.04	0.28	0.21	15.59

3.1.3. Mineral Phases of Binders

Figure 2 shows the diffractograms of CEM II. There is a reflection of quartz (SiO_2), wollastonite (Ca Si O_3), garnet (Ca, Fe, Mg) O Al, Fe . . .)), osumilite (K-Na-Ca-Mg-Fe-Al-Si), and calcite ($CaCO_3$). Osumilite mineral takes the most dominant phase of 19%, followed by garnet with 16% phase representation by weight. The presence of quartz mineral, which is mostly not affected by heat treatment [41], is seen in the diffractograms phase spectra at 6%. Wollastonite and calcite minerals were visible at 4% and 3% weight content, respectively. The two major chemical oxide components (calcium and silica oxides) presents osumilite as having good potential for cement production [42]. The result is coherent with the XRF data of CEM II studied here. Figure 3 shows the phase pattern view of the calcined RHA highlighting quartz (SiO_2), apatite (Ca_5 (F.Cl) P_3O_{12}), englishite (K_3 Na_2 Ca_{10} Al_{15} [PO_4]), and garnet 3(Ca, Fe, Mg) O. Al, Fe) as the mineral contents of the studied sample. The spectrum peak pattern can be described as apatite (13%) as the most dominant mineral present in the calcined RHA, followed by garnet and englishite with 4% mineral deposits. Quartz (SiO_2) has the lowest mineral peak phase of 3%. The XRD examination confirms the SiO_2 chemical oxide composition dominance in the XRF analysis. Thus, the result further revealed that calcining RHA up to 700 °C could produce an amorphous material (76%) suitable for concrete improvement.

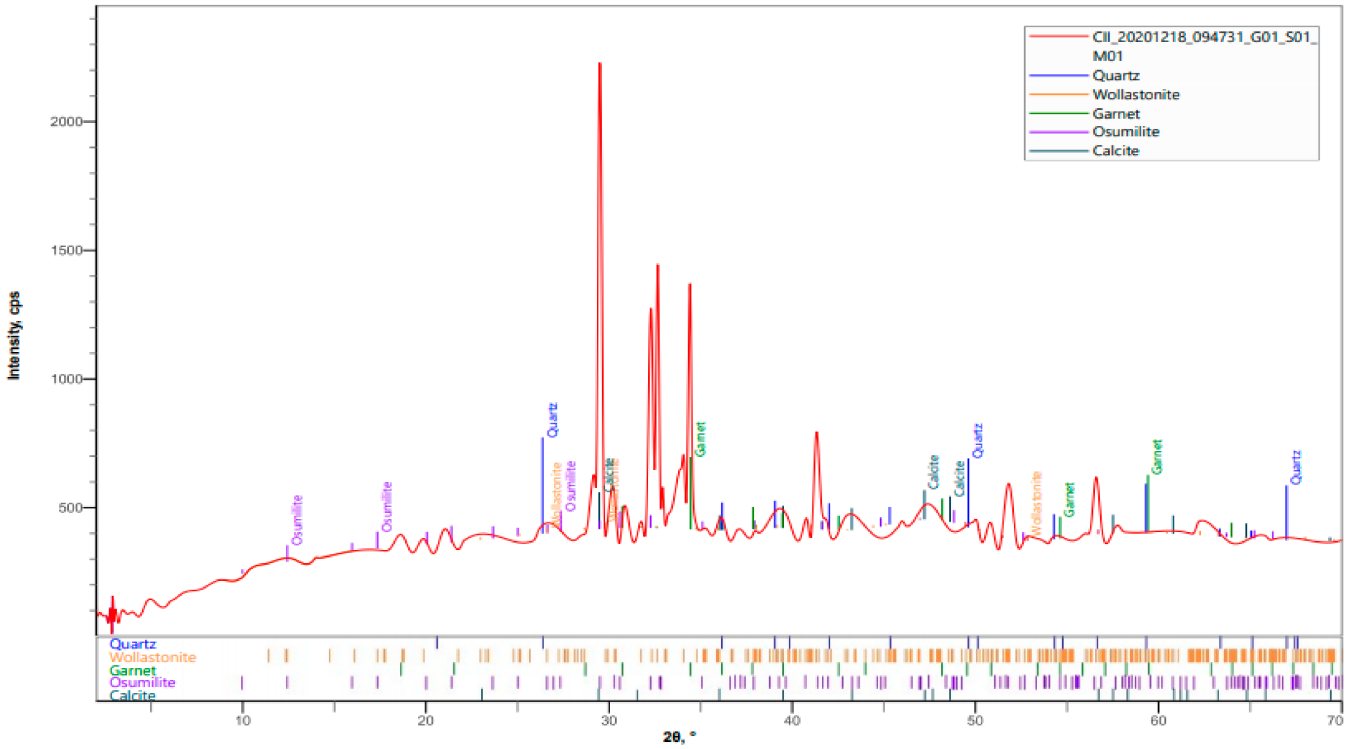

Figure 2. The XRD patterns of CEM II.

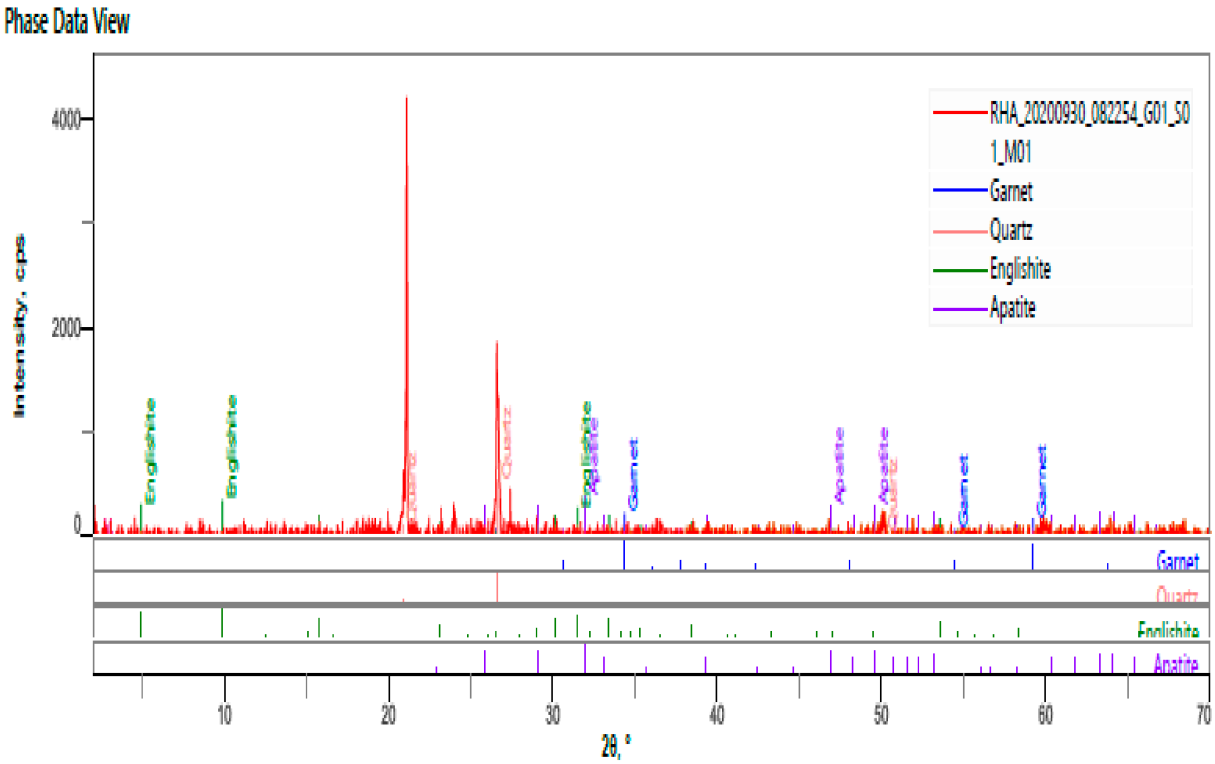

Figure 3. The XRD patterns RHA.

3.1.4. Morphology of Binders

The SEM images of the two binding materials put together (CEM II and RHA) are shown in Figures 4 and 5, respectively. Figure 4 projects the SEM images of CEM II used in this study when viewed at 100 µm and 200 µm magnification settings. The images are irregular, close to angular in shape, and interconnected. Micro-air space (dark spots, C) detaches the grains, prompting the specific grains to be recognised. The CEM II SEM image also indicated two grey band readings for particles (i.e., light grey, A and dark grey, B) portraying C_3S (alite) and C_2S (belite), respectively. The white spots represent the Fe^+ or Al^+ in C_3S or C_4AF. The results from the morphology of CEM II is consistent with Joshua et al. [43] SEM findings on major cement brands in Nigeria. The SEM image of the whitish RHA powder (Figure 5) particle at the same 100 µm and 200 µm magnifications also showed a smooth broad surface and slightly irregular shaped particles. The SEM image manifested dark grey and light grey irregular shapes indicated as G and H, respectively, in Figure 5.

3.1.5. FTIR/ATR of Binders

Figure 6 shows the FTIR/ATR transmittance spectra of anhydrite CEM II, 42.5 N. The IR bands at 712, 872, 910, 1111, 1420, 1685–1793, and 3381–3422 cm^{-1} emerged as a result of v_4—stretching of carbonate, v_2—out of plane vibration CO_3^{2-}, S–O stretching of SO_4^{2-}, v_3—asymmetric stretching of CO_3^{2-}, bending mode of water, presence of $CaCO_3$, and stretching of OH band, respectively [44]. The weak peak of 3422 cm^{-1} in the high zone highlights OH stretching of $Ca(OH)_2$, indicating a poor portlandite formation. The close absorption bands between 3381 and 3422 cm^{-1} in the FTIR spectra's peak region revealed that CEM II contains fewer water molecules. Figure 7 shows the IR spectra obtained from the calcined RHA characterised in this work. Peak identification was performed based on studies by Srivastava et al. [45] and Totlani et al. [46]. According to the authors, at 3709 and 2920 cm^{-1} bands, both free and hydrogen-bonded OH groups and Si–OH group on the adsorbent surface exist. The stretching arises due to the silanol groups (Si–OH) and

adsorbed water on the surface. The author pointed out that CO groups' transmittance of vibration in lactones occurs at 1050–1300 cm^{-1} bands. The presence of Si–H is usually at 793 and 469 cm^{-1} bands.

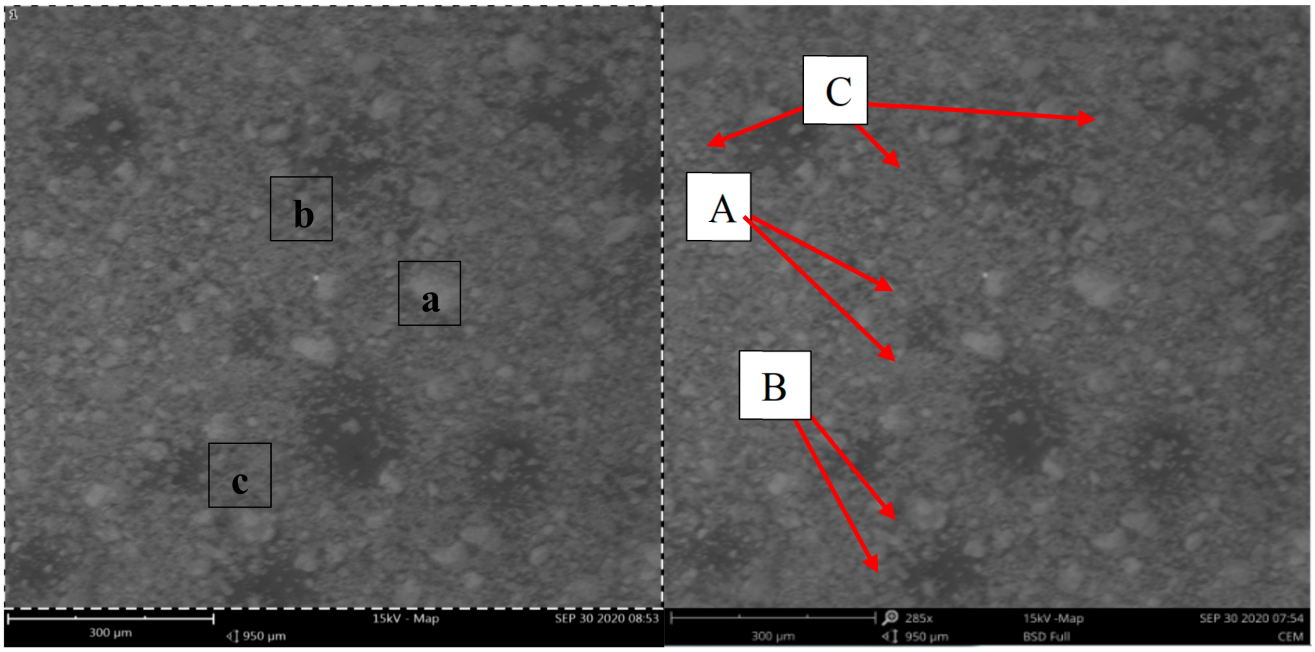

Figure 4. The SEM images of CEM II.

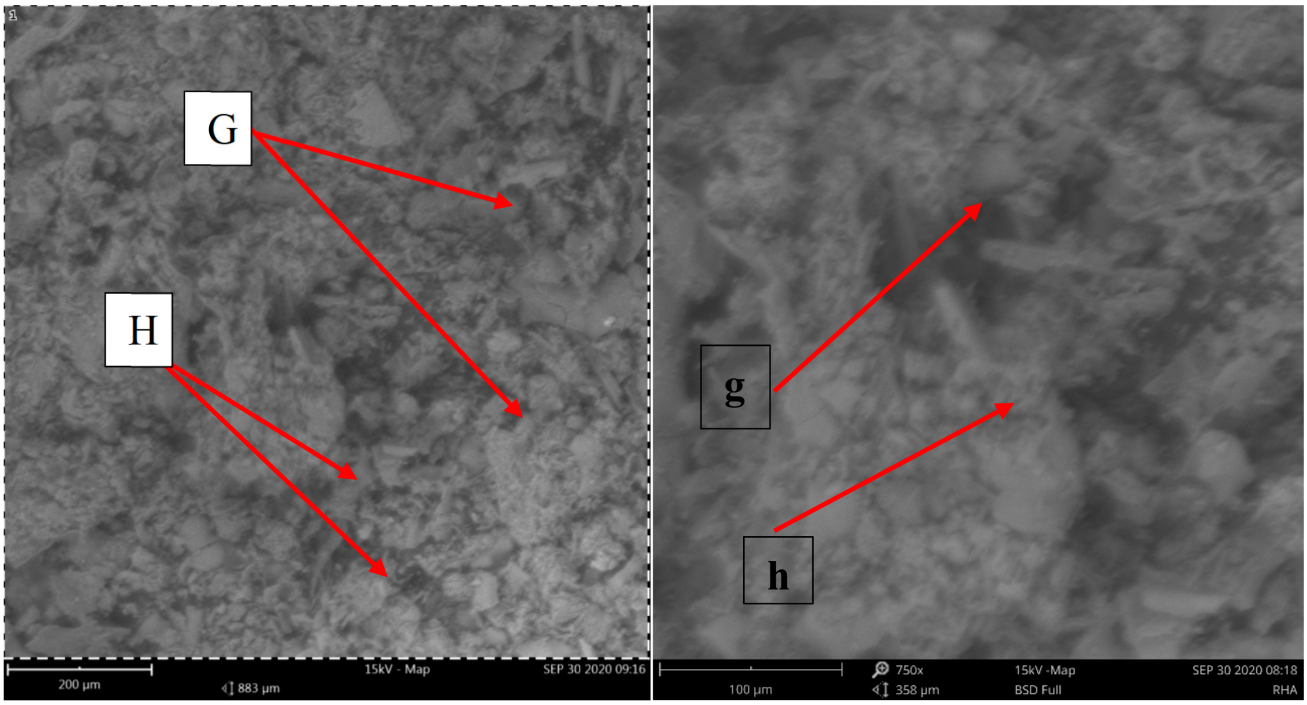

Figure 5. The SEM images of RHA.

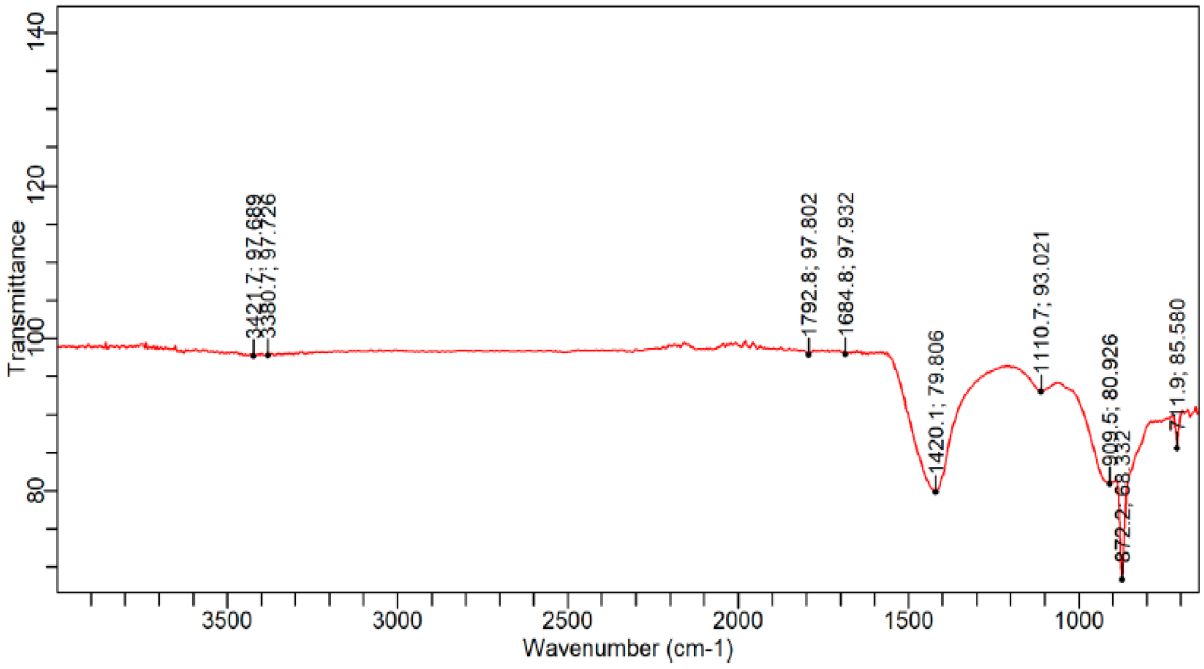

Figure 6. The FTIR/ATR spectra of CEM II.

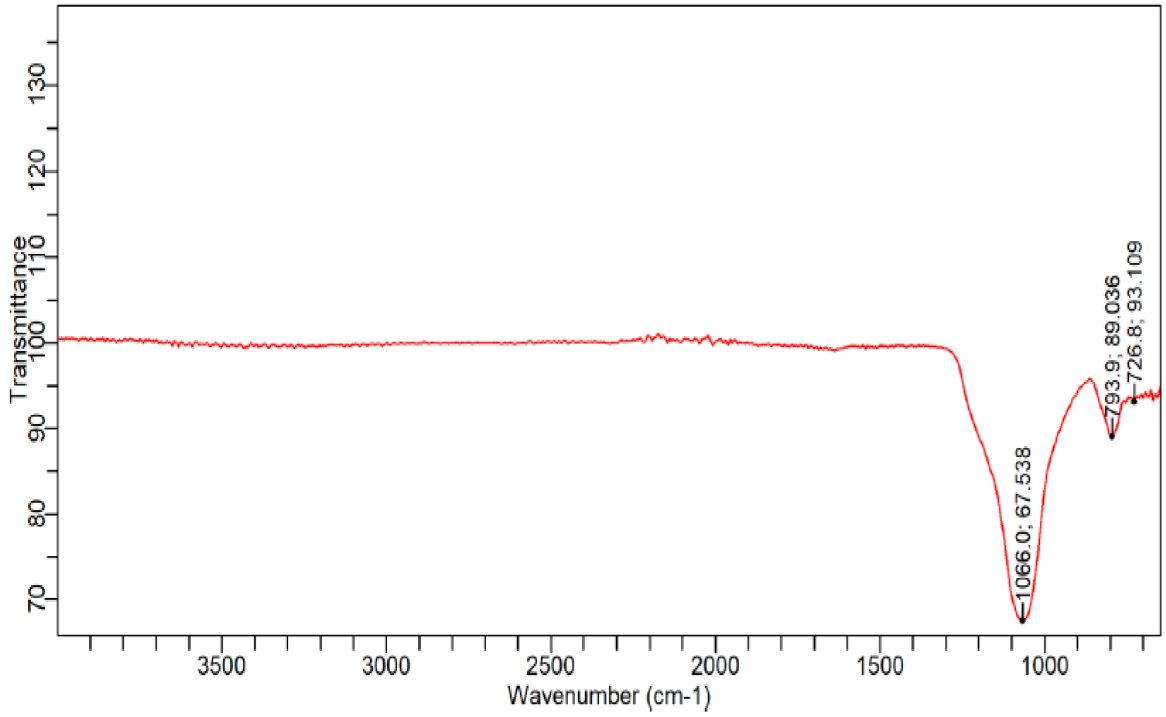

Figure 7. The FTIR/ATR spectra of RHA.

As shown in Figure 7, there appear to be steady transmittances of Si–OH groups, Si–CH–CH_2 stretch, and aromatic compounds (H–C), respectively, from 3700 to 1300 cm^{-1} bands. The peak of the 1066 cm^{-1} band may be attributed to CO groups' vibration transmittance in lactones. Finally, the presence of Si–H is seen at the transmittance peak of 793 cm^{-1} bands. All the spectra conform to those found in the literature [45–47].

3.2. Characterisation of Aggregates

The PSD plot in Figure 8 shows that the fine aggregate sample is medium sand of Shetty [48] group, whereas the coarse aggregate used for the study is uniformly graded stone. The physical characteristics of the fine and coarse aggregate are tabulated in Table 5 available in [11] study.The fine aggregate recorded fineness modulus (FM) of 2.87; coefficient of uniformity (Cu) of 2.39; coefficient of curvature (Cc) of 0.94; specific gravity (SG) of 2.65; and water absorption = 1.2% in the physical properties' tests. In the same vein, the coarse aggregate analysed for the study had a specific gravity of 2.7, water absorption of 1.05%, aggregate crushing, and impact values of 28% and 11%. These findings were expected and reinforced the usefulness of sieving out finer particles of the river sand with 300 µm sieves and washing coarse aggregate to minimise the dust content, which complied with requirements in the literature [25,49]. There are similarities in fineness modulus (2.87) and the specific gravity of sand (2.79) between the present study and those described by Mermerdaş et al. [50]. The particle size distributions of the fine and coarse aggregates in the present study are consistent with the description of aggregates used in Zhou et al. [51].

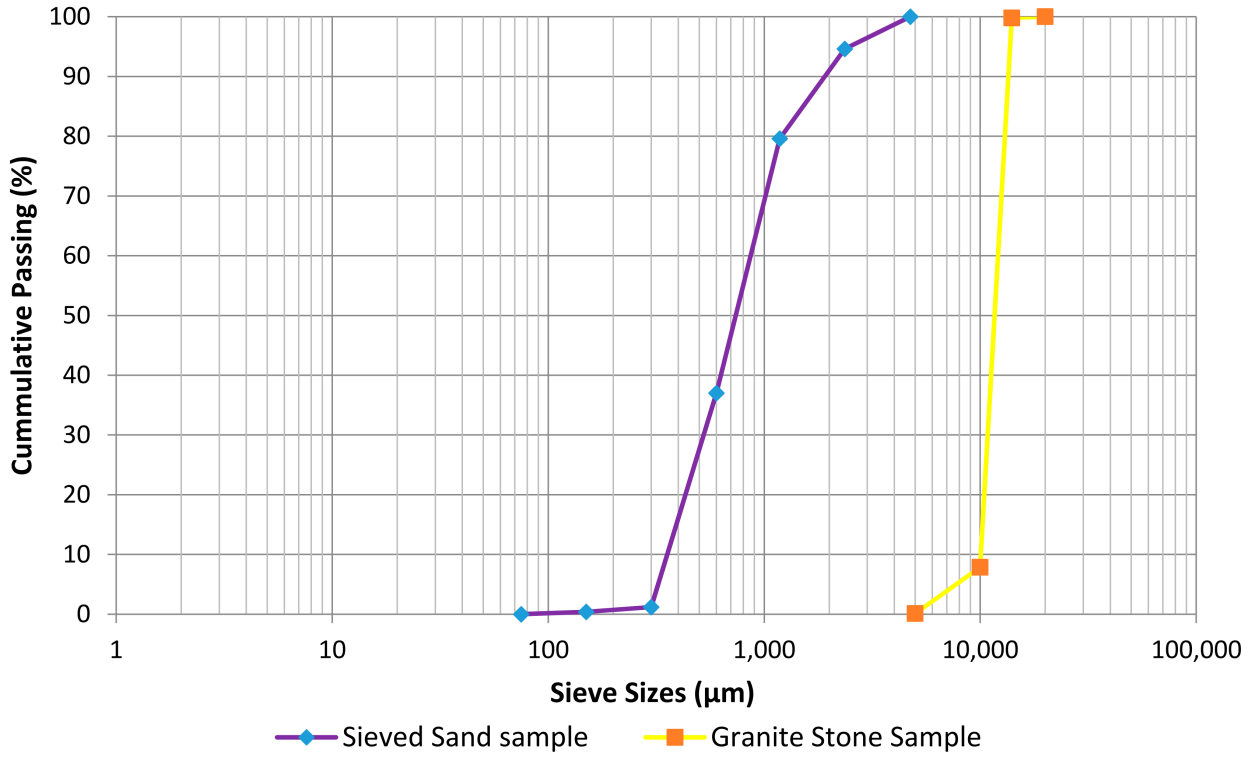

Figure 8. Particle size distribution of aggregates.

Table 5. Physical and mechanical properties of aggregates. (Nduka et al., 2021).

Material Properties	Fine Aggregate	Coarse Aggregate
Fineness modulus (FM)	2.87	-
Specific gravity (SG)	2.65	2.7
Water absorption, %	1.20	1.05
Aggregate crushing value, %	-	28
Aggregate impact value, %	-	11
D_{10}	360	10,000
D_{30}	540	11,000
D_{60}	860	13,000
C_u	2.39	1.30
C_c	0.94	0.93

3.3. Workability (Slump Flow)

The plot showing the observed slump flow values for the control and mixes containing RHA at various percentage replacements is presented in Figure 9. It can be observed from the figure that the slump flow for HPCs blended with RHA recorded increases of 4.81%, 8.65%, and 1.92% for RHAC-5, RHAC-10, and RHAC-15 mixtures, respectively, when compared to the control mixture. Additionally, RHAC-20, RHAC-25, and RHAC-30 had a reduced slump flow of 11.53%, 23.08%, and 39.42%. This phenomenon may be because the ground RHA had a particle size distribution similar to CEM II, so there was a high-water demand effect. The results from RHAC-5 to RHAC-20 are in conformance to the slump flow range of 450 mm–600 mm, as recommended by Neville [9]. An important issue emerging from these results is that HPC containing RHA as a cement substitute requires more water than the control mix to develop similar workability.

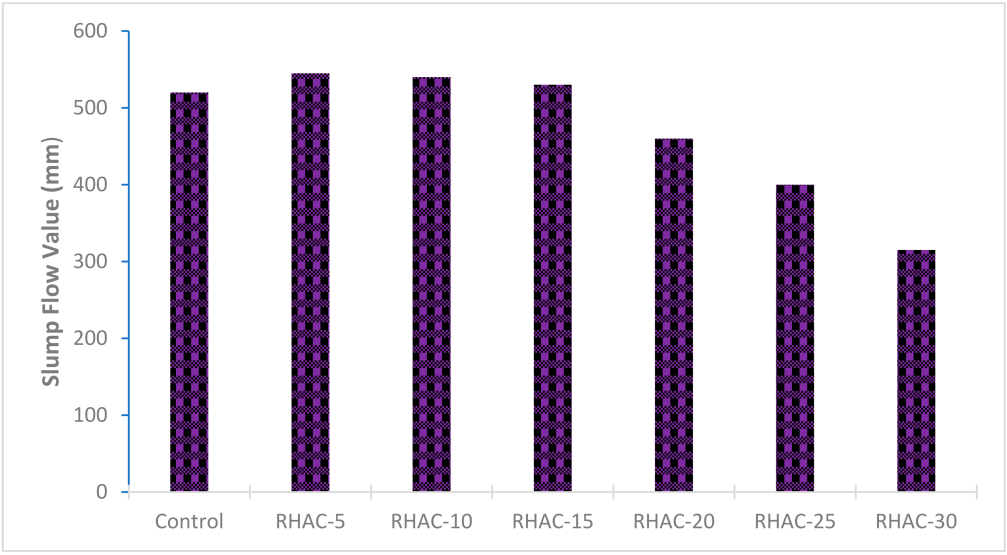

Figure 9. Slump flow of HPC made with different contents of RHA.

3.4. Durability Properties of RHA-Based HPC

3.4.1. Water Absorption of HPC

The average test results for the RHA blended HPCs' water absorption at 28, 56, and 90 days are illustrated in Figure 10. The water absorption varied in the ranges of 1.27–3.88% for 28 days, 2.80–5.62% for 56 days, and 2.50–5.13% for 90 days. Most findings are inconsonant with the acceptable range of water absorption for HPC, as pointed out by ASTM C 642 [52]. The standard specifies high-quality concrete to have water absorption in the range of 2–5%. Thomas [53] averred that low range water absorption in RHA based concrete is due to the limited pore connectivity and reduced porosity of the concretes. However, the water absorption of RHAC-30 was higher than the specified standard at 56 and 90 days, respectively. This increase may be related to the apparent porosity features of RHA. Once the apparent porosity of RHA based HPC increases, it is anticipated that water absorption will increase. The increase in water absorption of RHA based concrete is reported by Olutoge and Adesina [54] while relating the phenomenon to the hygroscopic nature of RHA material. As can be seen, there was a slight improvement at 90 day observations. All the RHA blended mixtures showed improvement at 90 days curing compared to the 56 days observation. The water absorption of the HPCs increased with a greater RHA content, as evident in all the RHA based HPCs at curing days. The control sample attained the lowest level of water absorption in all curing days. Usually, water absorption is affected by the water to cement ratio, the paste's content and volume in the concrete mix. In this light, water absorption will increase when the volume content of RHA increases.

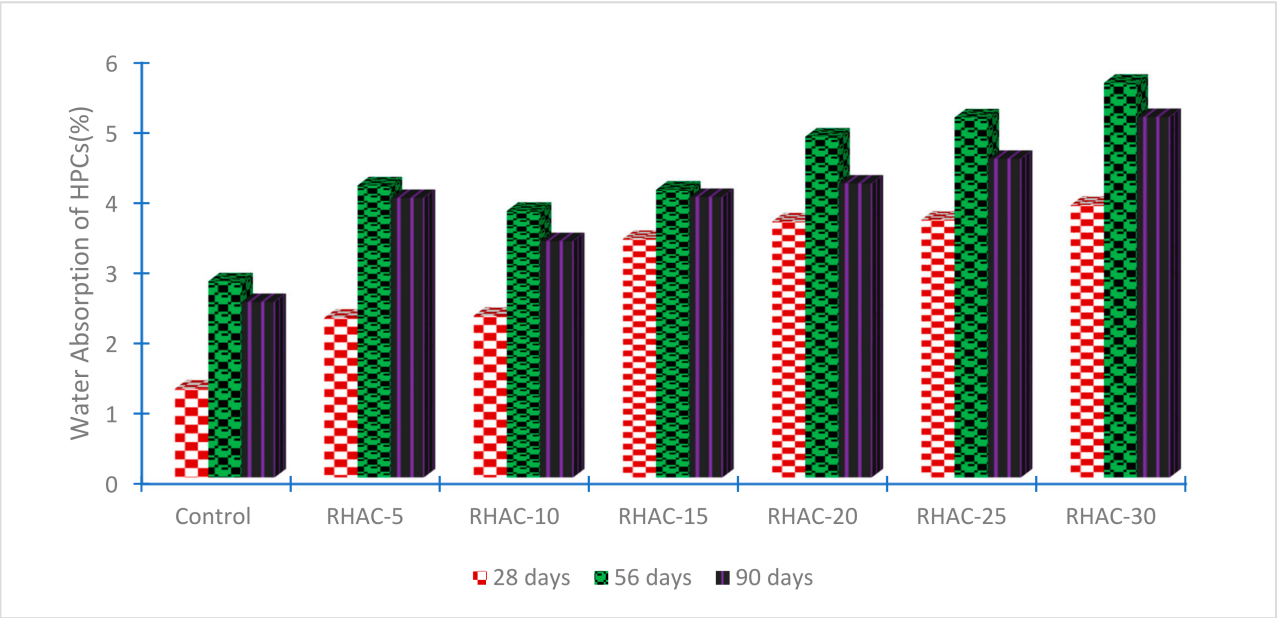

Figure 10. Water absorption development of HPCs incorporating RHA at different curing days.

3.4.2. Sorptivity of HPCs

The variations of water absorption by capillary pressure in relation to time passed are depicted in Figures 11–13. The absorption rate (sorptivity coefficient) graphs for RHA blended HPCs were computed between the change in weight per unit area over the unit weight of water and the period's square root (minutes).

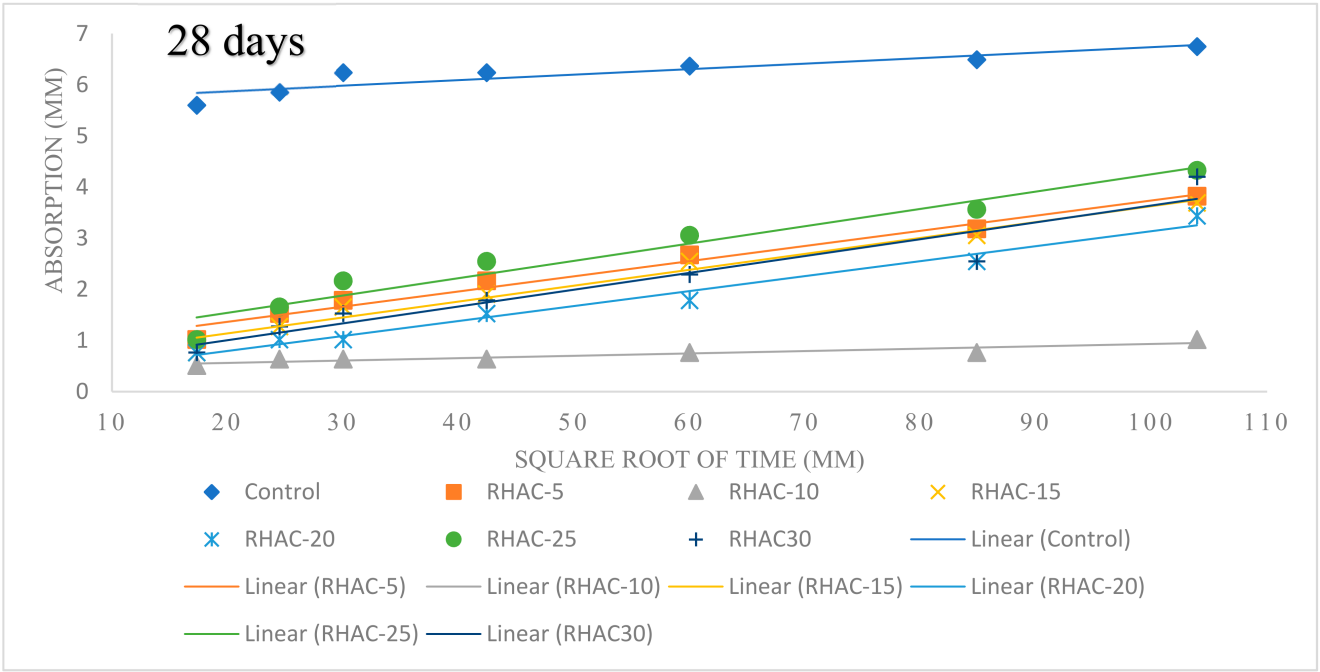

Figure 11. Sorptivity characteristics of HPCs with RHA for 28 days.

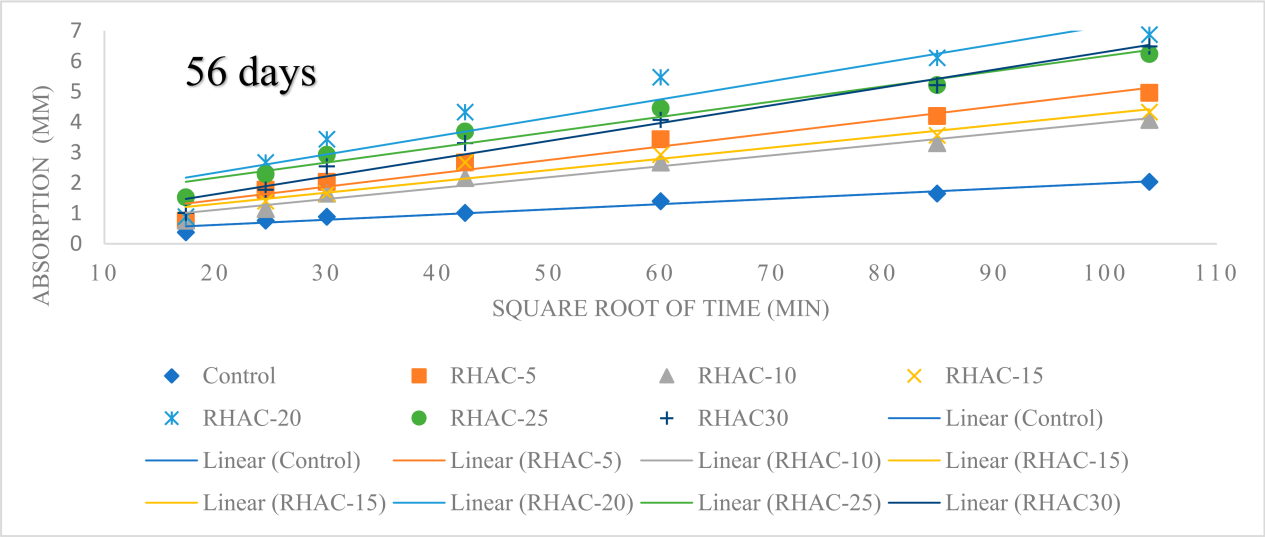

Figure 12. Sorptivity characteristics of HPCs with RHA for 56 days.

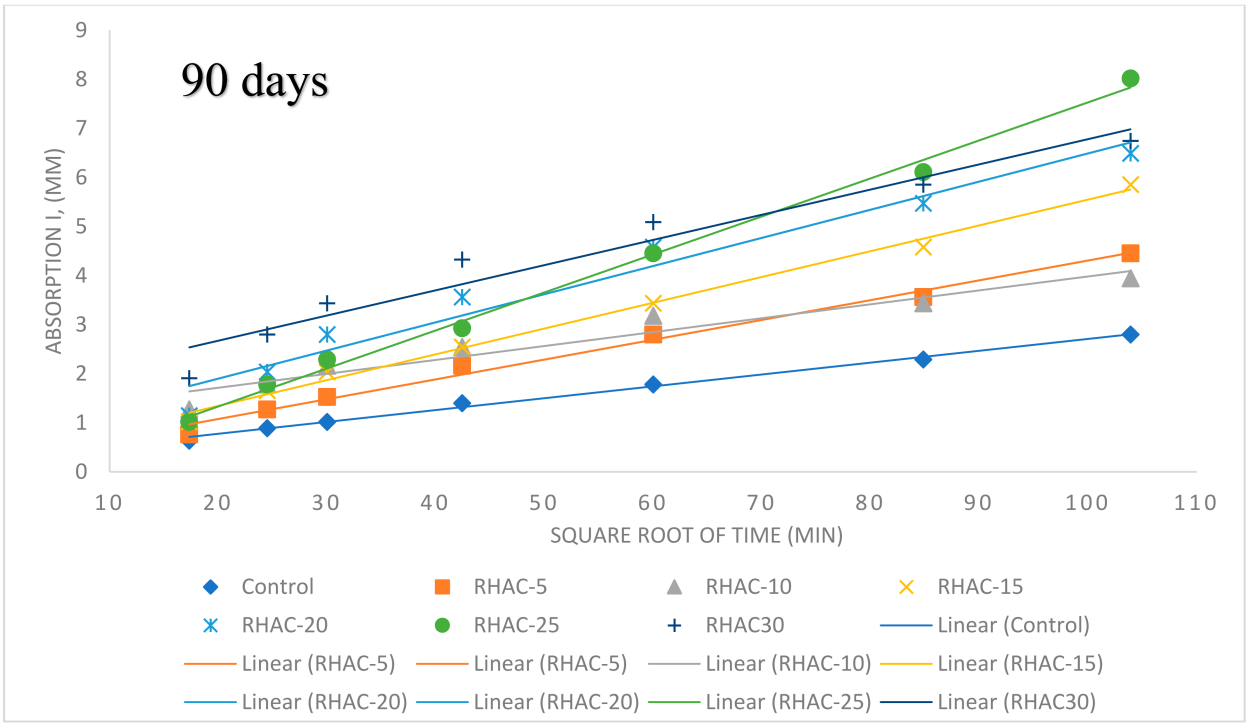

Figure 13. Sorptivity characteristics of HPCs with RHA for 90 days.

Figures 11–13 depict the effects of blended RHA on the water sorptivity of HPC at 28, 56, and 90 days. The capillary water action decreased as the curing days progressed for the control mix. The RHA blended mixtures water sorptivity fluctuated due to the RHA's pore structure, particle size distribution, and specific surface area affecting their microstructure and cement hydration. A 28-day CEM II had the highest water capillary ingress of approximately 5.5–6.4 mm over the 180 min inspection time. The RHA blended HPCs had an average water sorptivity of 2.93 mm, higher than that of the control mix (1 mm). A similar trend continued for 90 days; the average water ingress was computed to be 2.96 mm for the MCC blended HPCs.

The control at the same age had a lower water absorption value (0.44 mm) than the RHA blended mix. The 10% cement replacements at 28 and 56 days gave the best water

sorptivity values, supporting the mechanical properties results. These inconsistencies may be due to RHA's micro, macro, and mesoporous structure, which influenced its pozzolanic activity and specific surface area. The RHA blended matrix performed slightly more poorly in water sorptivity compared to the control mix. A reverse behaviour could be expected regarding a higher specific surface area, pore structure, and pore size distribution given in Table 4. The binary mix of cement (slightly finer than RHA) and calcined RHA is expected to yield a higher packing density in a granular mixture [55]. Therefore, this study's findings situate well with Vieira et al. [35], who studied the effects of various particle size distribution and replacement contents of RHA on the compressive strength of HPC.

Table 6 reports the correlation coefficient of RHA modified HPC at 28, 56, and 90 days. The control mix showed a near relationship between the rate of absorption and the square root of time at 28 days with a computed coefficient of correlation (R^2 = 0.83), whereas 56 and 90 days had close to insignificant coefficients of correlation (R^2 = 0.98 and 0.94, respectively). This finding is an indication of further hydration tendencies of the tested samples as curing days increased. The correlation coefficients were R^2 = 0.98, 0.96, 0.99; 0.88, 0.98, 0.94; 0.97, 0.95, 0.99; 0.98, 0.88, 0.96; 0.95, 0.96, 0.99 and 0.92, 0.98, 0.95, respectively, for RHAC-5, RHACC-10, RHACC-15, RHACC-20, RHACC-25, and RHACC-30, respectively. These data must be interpreted with caution because of their close relationships. ASTM C 1585 [30] pointed out that "If the data between 1 min and 6 h do not follow a linear relationship (a correlation coefficient of less than 0.98) and show a systematic curvature, the initial rate of absorption cannot be determined". The correlation coefficient of RHAC-5 was near significant in 28 and 56 days and significant at 90 days. RHAC-10 recorded a moderate significant difference at 28 days. MCCC-15 to MCCC-30 mixtures highlighted varied insignificant differences in the measured coefficient of correlation across the 28, 56, and 90 day tests. There are several possible explanations for this result. For example, Le and Ludwig [55] found that adding calcined RHA in cement matrix increases cement hydration due to their nucleation and dilution effects coupled with higher packing density in granular mixtures.

Table 6. Summary for sorptivity correlation coefficient of RHA blended HPCs.

Mix ID/Sorptivity Correlation Coefficient	28 Days	56 Days	90 Days
	R^2	R^2	R^2
Control	0.8252	0.9653	0.9955
RHAC-5	0.9770	0.9602	0.9899
RHAC-10	0.8682	0.9751	0.9361
RHAC-15	0.9728	0.9521	0.9939
RHAC-20	0.9800	0.8810	0.9612
RHAC-25	0.9497	0.9619	0.9955
RHAC-30	0.9180	0.9767	0.9476

3.4.3. Chemical Durability: Acid Attack, Sulphate Attack, and Chloride Attack on HPCs

Figures 14–17 show the 7, 28, 56, and 90 day compressive strength of hardened HPCs with the different replacement of cement by RHA exposure to acid, sulphate, and chlorine attacks.

From the figures, the control exhibited a compressive strength variation between 2.20 and 14.02% after 7, 28, 56, and 90 days of acid, sulphate, and chlorine solutions curing and compared with water immersion curing. There is a decrease in percentage compressive strength loss as the curing ages increase in the HPC control sample. At all the mix types, the chlorine environment showed a relatively high impact on the tested sample compressive strength. The RHAC-5 mixture exhibited a compressive strength drop between 10.59 and 22.02% after 7, 28, 56, and 90 days of acid, sulphate, and chlorine curing. Whereas for other mixes (RHAC-10 to RHAC-30), the compressive strength drops

between water and other chemical environments curing obtained was in the range of 2.83 to 9.81% at 7, 28, 56, and 90 days. HPCs containing RHA tend to show superior compressive strength reduction in the studied chemical environments. Analysing the results, it can be inferred that mesoporous RHA particles dominated the void areas in HPC, leading to reduced acid and sulphate attacks and chlorine migration into the matrix. The findings here complied with Thomas [53] on optimised 15–20% cement replacement with RHA capability of reducing acid attack and chloride penetration in concrete.

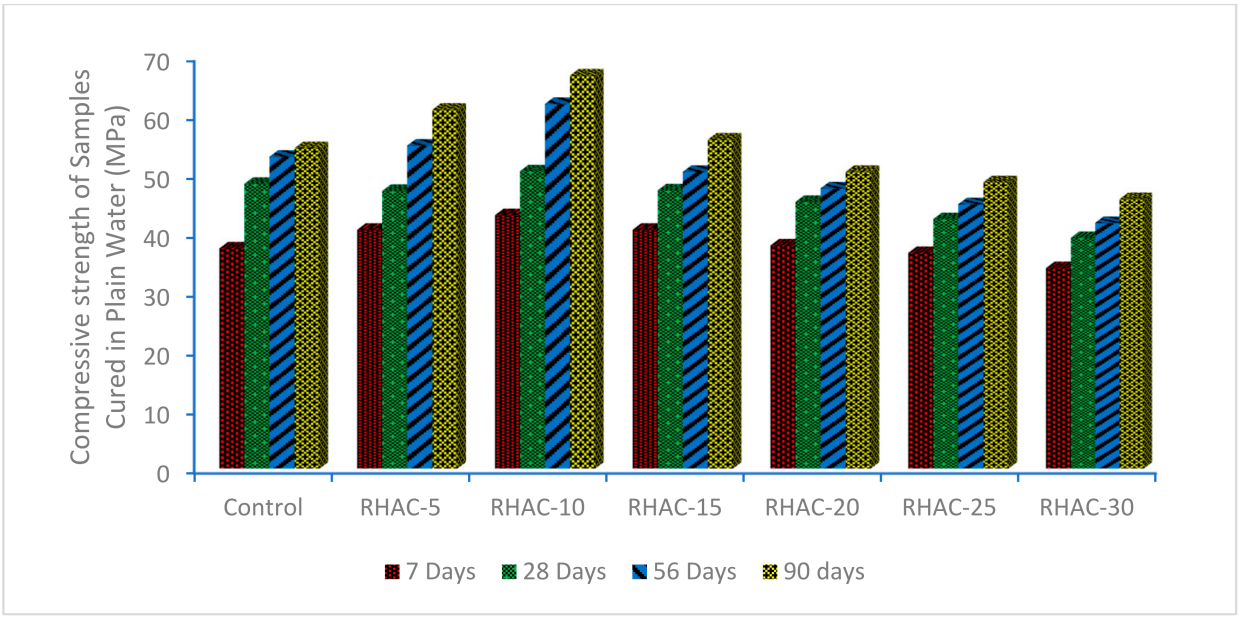

Figure 14. Compressive strength of RHA blended HPC cured in water.

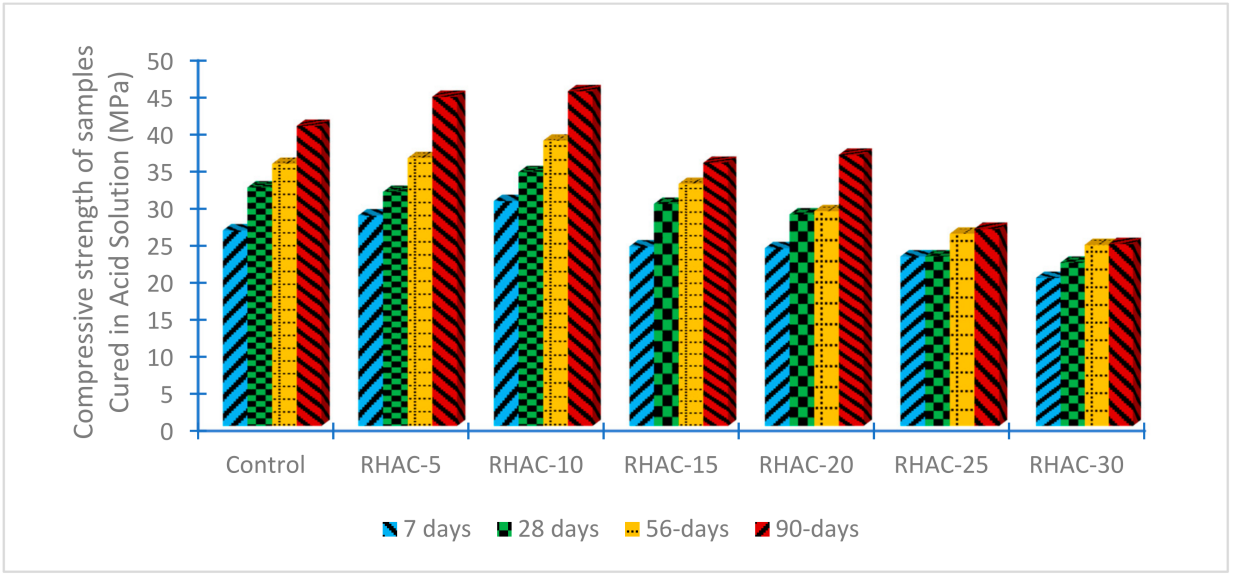

Figure 15. Compressive strength of RHA blended HPC cured in an acid environment.

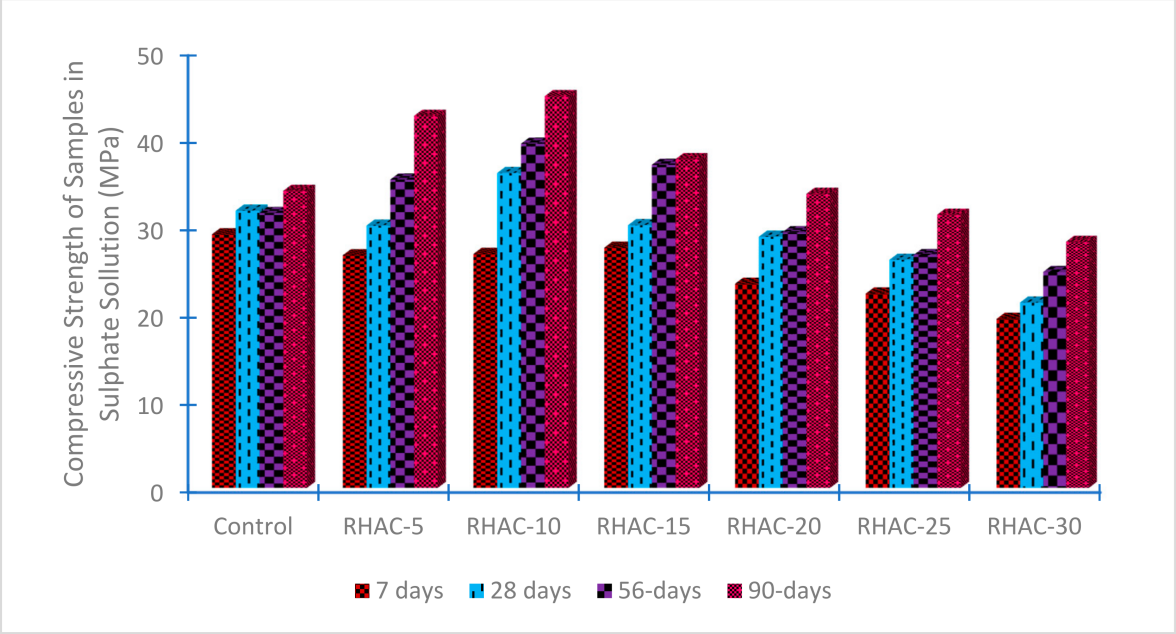

Figure 16. Compressive strength of RHA blended HPC cured in a sulphate environment.

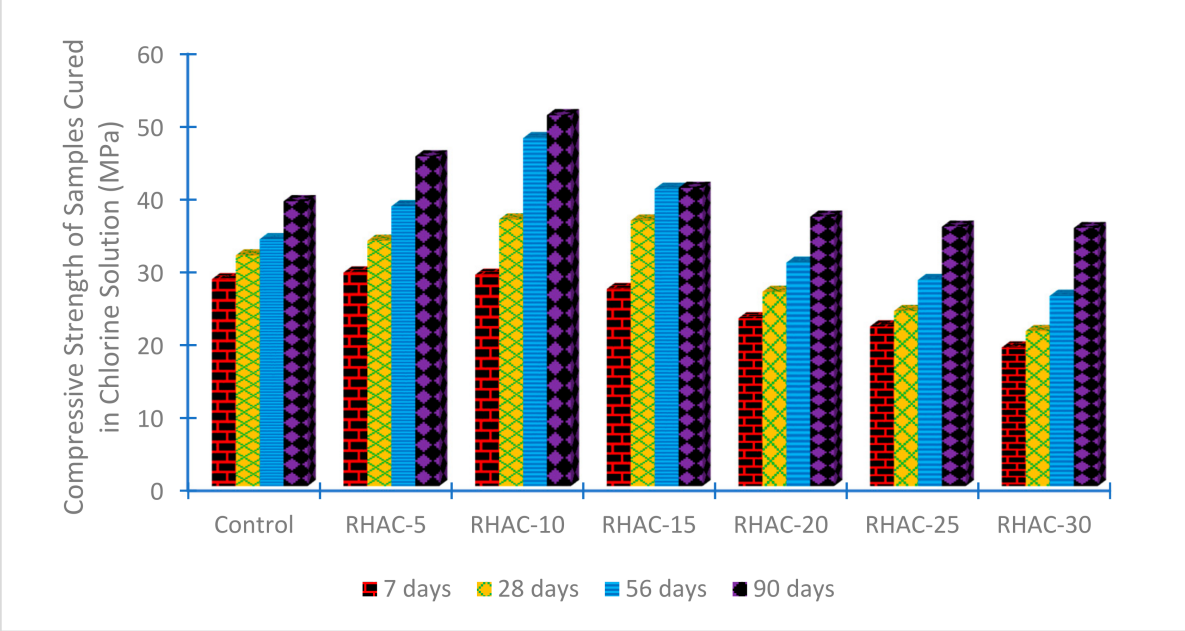

Figure 17. Compressive strength of RHA blended HPC cured in a chlorine environment.

4. Conclusions

The current paper examines the durability dimensions of water absorption, sorptivity, and chemical attack of an HPC blended with an agricultural by-product of RHA. CEM II was replaced at 5%, 10%, 15%, 20%, 25%, and 30% with RHA, having a constant 0.3 W/B and a 0.3% by weight of binder content of SAP in the HPC mixture. The plastic property of the mixture was evaluated using the slump flow test, and the results were compared with the propositions of Neville [9]. The following inferences are drawn from the research.

- The RHAC-5 to RHAC-20 are the only RHA based HPC that conformed to the slump flow range of 450 mm to 600 mm.

- The water absorption values obtained in RHA based HPCs are within the 2–5% acceptable range of water absorption for HPC, conforming to ASTM C 642 [52].
- The sorptivity correlation coefficients are less than or equal to 0.98 for RHA blended HPCs, conforming to ASTM C 1585-04 [30].
- Mesoporous RHA particles dominated the void areas in HPC, leading to reduced acid and sulphate attacks and chlorine migration into the HPC matrix.
- The chlorine environment at all the mix types showed a relatively high impact on the tested samples' compressive strengths.
- These findings validated that that locally produced RHA would have potential as a cement replacement in HPC.
- Subsequently, the RHA is an economical agro-waste; a scalable product of RHA would be a resource to sustainable technology.

Author Contributions: Conceptualisation, D.O.N.; methodology, D.O.N., B.J.O. and B.G.F.; investigation, D.O.N., B.J.O. and O.I.F.; writing—original draft preparation, D.O.N.; writing—review and editing, B.J.O., O.I.F. and B.G.F.; supervision, O.I.F. and B.J.O. All authors have read and agreed to the published version of the manuscript.

Funding: This paper received no external funding, and the APC was funded by Covenant University Center for Research, Innovation and Discovery (CUCRID).

Acknowledgments: The authors extend their appreciation to the suppliers of the superplasticiser-Masterglenium Sky 504—BASF Limited, West Africa; the Superabsorbent Polymers (SAP)—SNF Floerger-ZAC de Milieux, France, and 100 mm cube metal moulds—the Nigerian Building and Road Research Institute (NBRRI), Ota.

Conflicts of Interest: The authors declare no conflict of interest.

References

1. Raiden, A.; King, A. Social value, organisational learning, and the sustainable development goals in the built environment. *Resour. Conserv. Recycl.* **2021**, *172*, 105663. [CrossRef]
2. Rheude, F.; Kondrasch, J.; Röder, H.; Fröhling, M. Review of the terminology in the sustainable building sector. *J. Clean. Prod.* **2020**, *286*, 125445. [CrossRef]
3. Adekoya, F. Nigeria's Cement Capacity Hits 60 MMT. The Guardian Business Online News. 2020. Available online: https://guardian.ng/business-services/nigerias-cement-capacity-hits-60mmt-2022/ (accessed on 30 December 2020).
4. Oyebisi, S.; Ede, A.; Olutoge, F.; Omole, D. Geopolymer concrete incorporating agro-industrial wastes: Effects on mechanical properties, microstructural behaviour and mineralogical phases. *Constr. Build. Mater.* **2020**, *256*, 119390. [CrossRef]
5. Schmid, M.; Plank, J. Dispersing performance of different kinds of polycarboxylate (PCE) superplasticizers in cement blended with a calcined clay. *Constr. Build. Mater.* **2020**, *258*, 119576. [CrossRef]
6. Zhang, Z.; Liu, S.; Yang, F.; Weng, Y.; Qian, S. Sustainable high strength, high ductility engineered cementitious composites (ECC) with substitution of cement by rice husk ash. *J. Clean. Prod.* **2021**, *317*, 128379. [CrossRef]
7. Hossain, M.; Karim, M.; Elahi, M.; Islam, M.; Zain, M. Long-term durability properties of alkali-activated binders containing slag, fly ash, palm oil fuel ash and rice husk ash. *Constr. Build. Mater.* **2020**, *251*, 119094. [CrossRef]
8. ACI THPC/TAC. *ACI Defines High-Performance Concrete (The Technical Activities Committee Report (Chairman—H.G. Russell)*; American Concrete Institute: Farmington Hills, MI, USA, 1999.
9. Neville, A.M. *Properties of Concrete*, 5th ed.; Pearson Educational Limited: London, UK, 2012. Available online: https://www.pearson.com/uk/educators/higher-education-educators/program/Neville-Properties-of-Concrete-Properties-of-Concrete-5th-Edition/PGM1001873.html (accessed on 30 December 2020).
10. Aïtcin, P.C. *High-Performance Concrete*; Taylor & Francis e-Library: New York, NY, USA, 2004. [CrossRef]
11. Nduka, D.O.; Olawuyi, B.J.; Fagbenle, O.I.; Fonteboa, B.G. Effect of $K_yAl_4(Si_{8-y})O_{20}(OH)_4$ Calcined Based-Clay on the Microstructure and Mechanical Performances of High-Performance Concrete. *Crystals* **2021**, *11*, 1152. [CrossRef]
12. Faleschini, F.; Ruiz, M.A.F.; Zanini, M.A.; Brunelli, K.; Pellegrino, C.; Hernández-Montes, E. High performance concrete with electric arc furnace slag as aggregate: Mechanical and durability properties. *Constr. Build. Mater.* **2015**, *101*, 113–121. [CrossRef]
13. Harbec, D.; Zidol, A.; Tagnit-Hamou, A.; Gitzhofer, F. Mechanical and durability properties of high performance glass fume concrete and mortars. *Constr. Build. Mater.* **2017**, *134*, 142–156. [CrossRef]
14. Rumman, R.; Bari, M.; Manzur, T.; Kamal, M.; Noor, M. A Durable Concrete Mix Design Approach using Combined Aggregate Gradation Bands and Rice Husk Ash Based Blended Cement. *J. Build. Eng.* **2020**, *30*, 101303. [CrossRef]
15. Wang, J.; Xiao, J.; Zhang, Z.; Han, K.; Hu, X.; Jiang, F. Action mechanism of rice husk ash and the effect on main performances of cement-based materials: A review. *Constr. Build. Mater.* **2021**, *288*, 123068. [CrossRef]

16. Okpiaifo, G.; Durand-Morat, A.; West, G.H.; Nalley, L.L.; Nayga, R.M.; Wailes, E.J. Consumers' preferences for sustainable rice practices in Nigeria. *Glob. Food Secur.* **2019**, *24*, 100345. [CrossRef]
17. Ugbede, F.O.; Osahon, O.D.; Akpolile, A.F.; Oladele, B.B. Assessment of heavy metals concentrations, soil-to-plant transfer factor and potential health risk in soil and rice samples from Ezillo rice fields in Ebonyi State, Nigeria. *Environ. Nanotechnol. Monit. Manag.* **2021**, *16*, 100503. [CrossRef]
18. Sahoo, S.; Parhi, P.K.; Panda, B.C. Durability properties of concrete with silica fume and rice husk ash. *Clean. Eng. Technol.* **2021**, *2*, 100067. [CrossRef]
19. De Silva, G.S.; Vishvalingam, S.; Etampawala, T. Effect of waste rice husk ash from rice husk fuelled brick kilns on strength, durability and thermal performances of mortar. *Constr. Build. Mater.* **2020**, *268*, 121794. [CrossRef]
20. Adnan, Z.S.; Ariffin, N.F.; Mohsin, S.M.S.; Lim, N.H.A.S. Review paper: Performance of rice husk ash as a material for partial cement replacement in concrete. *Mater. Today Proc.* **2021**, in press. [CrossRef]
21. Hu, L.; He, Z.; Shao, Y.; Cai, X.; Zhang, S. Microstructure and properties of sustainable cement-based materials using combustion treated rice husk ash. *Constr. Build. Mater.* **2021**, *294*, 123482. [CrossRef]
22. Swaminathen, A.; Kumar, C.V.; Ravi, S.R.; Debnath, S. Evaluation of strength and durability assessment for the impact of Rice Husk ash and Metakaolin at High Performance Concrete mixes. *Mater. Today Proc.* **2021**, *47*, 4584–4591. [CrossRef]
23. EN, B. 197-1. *Cement, Composition, Specifications and Conformity Criteria for Common Cements*; British Standard Institution (BSI): London, UK, 2011. Available online: http://106.38.59.21:8080/userfiles/d46365fdde004ea0a5da5d9701142815/files/teckSolution/2019/10/EN%20197-1-2011_3750.pdf (accessed on 5 March 2020).
24. *Nigeria Industrial Standard [NIS] 444-1 Composition, Specification and Conformity Criteria for Common Cements*; Standards Organization of Nigeria: Abuja, Nigeria, 2018. Available online: https://standards.lawnigeria.com/2019/07/18/nigerian-standards-for-construction-materials-and-building-manufacturing-engineering/ (accessed on 13 June 2021).
25. Aïtcin, P.C. *High Performance Concrete*; CRC Press: Boca Raton, FL, USA, 1998. Available online: https://pdfcoffee.com/high-performance-concrete-5-pdf-free.html (accessed on 5 March 2020).
26. Olawuyi, B.J.; Boshoff, W.P. Influence of superabsorbent polymer on the splitting tensile strength and fracture energy of high-performance concrete. *MATEC Web Conf.* **2018**, *199*, 11004. [CrossRef]
27. BS EN 1008. *Mixing Water for Concrete: Specification for Sampling, Testing and Assessing the Suitability of Water, including Water Recovered from Processes in the Concrete Industry as Mixing Water for Concrete*; British Standards Institution: London, UK, 2002. Available online: https://standards.iteh.ai/catalog/standards/cen/8ab1a0fa-b727-48f7-9b31-739eba3732ca/en-1008-2002 (accessed on 10 June 2021).
28. Olawuyi, B.J. The Mechanical Behaviour of High-Performance Concrete with Superabsorbent Polymers (SAP). Ph.D. Thesis, University of Stellenbosch, Stellenbosch, South Africa, 2016. Available online: https://scholar.sun.ac.za/handle/10019.1/98352 (accessed on 15 June 2021).
29. Mehta, P.K.; Monteiro, P.J. *Concrete: Microstructure, Properties, and Materials*; McGraw-Hill Education: New York, NY, USA, 2014.
30. ASTM C1585-13. *Standard Test Method for Measurement of Rate of Absorption of Water by Hydraulic-Cement Concretes, ASTM International*; ASTM: West Conshohocken, PA, USA, 2013. Available online: https://www.astm.org/c1585-13.html (accessed on 10 June 2021).
31. EN, B. 1097-6. *Tests for Mechanical and Physical Properties of Aggregates Part 6: Determination of Particle Density and Water Absorption*; BSI Standards Ltd.: Brussels, Belgium, 2013. Available online: https://standards.iteh.ai/catalog/standards/cen/efd7df30-eac1-4445-90eb-9b2958fb2564/en-1097-6-2013 (accessed on 10 June 2021).
32. EN, B. 12390-3: 2019. Testing Hardened Concrete. In *Compressive Strength of Test Specimens*; British Standard Institute: London, UK, 2019. Available online: https://standards.iteh.ai/catalog/standards/cen/7eb738ef-44af-436c-ab8e-e6561571302c/en-12390-3-2019 (accessed on 10 June 2021).
33. ASTM C267–20. *Standard Test Methods for Chemical Resistance of Mortars, Grouts, and Monolithic Surfacings and Polymer Concretes*; ASTM International: West Conshohocken, PA, USA, 2020. [CrossRef]
34. International Union of Testing and Research Laboratories for Materials and Structures (RILEM). *CPC4—Compressive Strength of Concrete 1975, TC14-CPC, RILEM Technical Recommendations for the Testing and Use of Construction Materials*; E & FN SPON: Oxford, UK, 1994; pp. 17–18. Available online: https://www.rilem.net/publication/publication/4?id_papier=3947 (accessed on 15 June 2021).
35. Vieira, A.P.; Filho, R.D.T.; Tavares, L.; Cordeiro, G.C. Effect of particle size, porous structure and content of rice husk ash on the hydration process and compressive strength evolution of concrete. *Constr. Build. Mater.* **2019**, *236*, 117553. [CrossRef]
36. Kwan, W.H.; Wong, Y.S. Acid leached rice husk ash (ARHA) in concrete: A review. *Mater. Sci. Energy Technol.* **2020**, *3*, 501–507. [CrossRef]
37. ASTM C618–15. *Standard Specification for Coal Fly Ash and Raw or Calcined Natural Pozzolan for Use in Concrete. Annual Book of ASTM Standards*; ASTM International: West Conshohocken, PA, USA, 2015.
38. Laidani, Z.E.-A.; Benabed, B.; Abousnina, R.; Gueddouda, M.K.; Kadri, E.-H. Experimental investigation on effects of calcined bentonite on fresh, strength and durability properties of sustainable self-compacting concrete. *Constr. Build. Mater.* **2019**, *230*, 117062. [CrossRef]

39. Newman, J.; Choo, B.S. *Advanced Concrete Technology Constituent Materials*; Butterworth-Heinemann: Oxford, UK, 2003. Available online: https://www.docme.su/doc/1273244/john-newman-b-s-choo---advanced-concrete-technology-1--co (accessed on 20 June 2021).
40. Mosaberpanah, M.A.; Umar, S.A. Utilizing Rice Husk Ash as Supplement to Cementitious Materials on Performance of Ultra High Performance Concrete:—A review. *Mater. Today Sustain.* **2020**, *7*, 100030. [CrossRef]
41. Danner, T.; Norden, G.; Justnes, H. Characterisation of calcined raw clays suitable as supplementary cementitious materials. *Appl. Clay Sci.* **2018**, *162*, 391–402. [CrossRef]
42. Saxena, S.; Kumar, M.; Chundawat, D.; Singh, N. Utilization of wollastonite in cement manufacturing. *Mater. Today Proc.* **2020**, *29*, 733–737. [CrossRef]
43. Opeyemi, J.; Olusola, K.O.; Fagbenle, O.I.; Ogunde, A.O.; Nduka, D.O. Assessment of Concrete Durability in Buildings: The Effects of the Quality of Cements Available in Lagos, Nigeria. *Int. Rev. Civ. Eng.* **2019**, *10*, 73. [CrossRef]
44. Jose, A.; Nivitha, M.; Krishnan, M.; Robinson, R. Characterization of cement stabilized pond ash using FTIR spectroscopy. *Constr. Build. Mater.* **2020**, *263*, 120136. [CrossRef]
45. Srivastava, V.C.; Mall, I.D.; Mishra, I.M. Characterization of mesoporous rice husk ash (RHA) and adsorption kinetics of metal ions from aqueous solution onto RHA. *J. Hazard. Mater.* **2006**, *134*, 257–267. [CrossRef]
46. Totlani, K.; Mehta, R.; Mandavgane, S. Comparative study of adsorption of Ni (II) on RHA and carbon embedded silica obtained from RHA. *Chem. Eng. J.* **2012**, *181–182*, 376–386. [CrossRef]
47. Sembiring, S. Preliminary Study on Functional Groups Characteristics of Asphalt Containing Rice Husk Silica. *J. Technomaterials Physic.* **2019**, *1*, 61–66. Available online: https://talenta.usu.ac.id/index.php/JoTP (accessed on 10 June 2021). [CrossRef]
48. Shetty, M.S. *Concrete Technology—Theory and Practice*; S. Chand and Company Limited Technology: New Delhi, India; Cement and Concrete Institute: Midrand, South Africa, 2004; pp. 219–228. Available online: https://www.schandpublishing.com/books/tech-professional/civil-engineering/concrete-technology-theory-practice/9789352533800/ (accessed on 20 July 2021).
49. Addis, B.; Goodman, J. Concrete mix design. In *Fulton's Concrete Technology*, 9th ed.; Owens, G., Ed.; Cement and Concrete Institute: Midrand, South Africa, 2009. Available online: https://www.scirp.org/(S(vtj3fa45qm1ean45vvffcz55))/reference/ReferencesPapers.aspx?ReferenceID=1480122 (accessed on 20 July 2021).
50. Mermerdaş, K.; Gesoglu, M.; Güneyisi, E.; Özturan, T. Strength development of concretes incorporated with metakaolin and different types of calcined kaolins. *Constr. Build. Mater.* **2012**, *37*, 766–774. [CrossRef]
51. Zhou, D.; Wang, R.; Tyrer, M.; Wong, H.; Cheeseman, C. Sustainable infrastructure development through use of calcined excavated waste clay as a supplementary cementitious material. *J. Clean. Prod.* **2017**, *168*, 1180–1192. [CrossRef]
52. ASTM C642-13. *Density, Absorption, and Voids in Hardened Concrete*; ASTM International: West Conshohocken, PA, USA, 2006. Available online: https://standards.globalspec.com/std/1581024/astm-c642 (accessed on 25 July 2021).
53. Thomas, B.S. Green concrete partially comprised of rice husk ash as a supplementary cementitious material—A comprehensive review. *Renew. Sustain. Energy Rev.* **2018**, *82*, 3913–3923. [CrossRef]
54. Olutoge, F.A.; Adesina, P.A. Effects of rice husk ash prepared from charcoal-powered incinerator on the strength and durability properties of concrete. *Constr. Build. Mater.* **2018**, *196*, 386–394. [CrossRef]
55. Le, H.T.; Ludwig, H.-M. Effect of rice husk ash and other mineral admixtures on properties of self-compacting high performance concrete. *Mater. Des.* **2016**, *89*, 156–166. [CrossRef]